

Article

Design Procedure Based on Maximum Efficiency for Wireless Power Transfer Battery Chargers with Lightweight Vehicle Assembly

Mattia Simonazzi * , Alessandro Campanini , Leonardo Sandrolini  and Claudio Rossi 

Department of Electrical, Electronic, and Information Engineering, University of Bologna, 40136 Bologna, Italy; alessandro.campanini@unibo.it (A.C.); leonardo.sandrolini@unibo.it (L.S.); claudio.rossi@unibo.it (C.R.)

* Correspondence: mattia.simonazzi2@unibo.it; Tel.: +39-051-2093040

Abstract: This paper analyzes two different design procedures for a series-parallel compensated WPT battery charger, based on different definitions of the operating resonant frequency in the condition of maximum link efficiency. The behaviour of the voltage gain magnitude and the input impedance angle of the resulting WPT links is studied for different loads and coupling coefficients. The design algorithms are supported by analytical formulas derived from an exact circuit analysis of the WPT link, avoiding approximations as far as possible. To support the theoretical approach a case study is proposed, in which both design procedures are implemented considering specifications in line with the actual automotive standards. To conclude, a characterization of the efficiency in both cases is derived.

Keywords: wireless power transfer; inductive power transfer; battery charger; design procedure



Citation: Simonazzi, M.; Campanini, A.; Sandrolini, L.; Rossi, C. Design Procedure Based on Maximum Efficiency for Wireless Power Transfer Battery Chargers with Lightweight Vehicle Assembly. *Energies* **2022**, *15*, 70. <https://doi.org/10.3390/en15010070>

Academic Editor: Byoung Kuk Lee

Received: 5 November 2021

Accepted: 9 December 2021

Published: 22 December 2021

Publisher's Note: MDPI stays neutral with regard to jurisdictional claims in published maps and institutional affiliations.



Copyright: © 2021 by the authors. Licensee MDPI, Basel, Switzerland. This article is an open access article distributed under the terms and conditions of the Creative Commons Attribution (CC BY) license (<https://creativecommons.org/licenses/by/4.0/>).

1. Introduction

Nowadays, environmental issues and technological improvements have pushed towards the direction of investing in electric mobility. The last frontier of power electronics and modern Li-ion batteries have made battery electric vehicles (BEV) and plug-in electric vehicles (PHEV) an efficient, low polluting and reliable alternative to traditional vehicles fed by fossil fuels. However, both BEV and PHEV suffer from problems related to the charging time and therefore charging at high power rating becomes fundamental. The charging problem is further aggravated when operating in harsh environments. Moreover, dangerous limitations of on-board chargers (OBCs) refer to safety of operation, reliability and need to manually connect the car to a charging station. To overcome these limitations, Wireless Power Transfer (WPT) systems have become an hot-spot to be further analyzed [1–3]. A typical DC/DC stage for a WPT system is split into two parts according to their positions either on- or off-board the vehicle. The off-board layout mounted on the ground assembly (GA) starts from the rectified DC bus voltage, V_{DC} , which is provided by the AC/DC stage. Then, it goes through the full-bridge inverter, that feeds the primary resonant tank, up to the primary transmitter coil. The receiver coil, positioned at the bottom of the car, is the first on-board component of the vehicle assembly (VA). It is directly connected to a secondary resonant tank and to a full-bridge diode rectifier [1,2]. Inside the car, an additional DC/DC converter takes care of charging the battery pack by means of a proper algorithm control able to track the constant-current-constant-voltage (CC-CV) charging cycle. The whole DC/DC stage is shown in Figure 1.

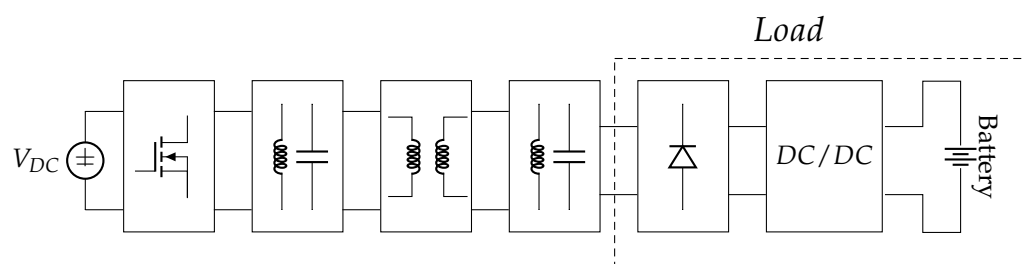


Figure 1. DC/DC power conversion stage for a WPT battery charger system, starting from the rectified voltage up to the load.

In addition, improper charging cycles that exceed upper and lower bounds along with battery usage result in an increase of the battery internal resistance (resistance growth) and in a decrease of the battery rated capacity (capacity fade). Therefore, it becomes necessary to estimate the battery State of Health (SOH) [4] from cell-level tests. The battery capacity can also be monitored through Data-Driven methods with the aim to assess the remaining useful life (RUL) [5]. Depending on the desired characteristics, several combinations of primary and secondary resonant circuits are available and analyzed in literature [6]. Basic resonant topologies, such as series-series (SS) and series-parallel (SP), have been deeply studied and compared [7]. Parallel-series (PS) and parallel-parallel (PP) are not of interest for battery charging applications, since the voltage applied to the tank is imposed by the inverter and an additional inductor must be connected in series between the inverter output port and the resonant tank [8], whose value may not be negligible.

A procedure design for the SS topology is given in [9,10] and what turns out is its relatively simple design, but with some difficulties in following the CC-CV charging cycle together with achieving zero-phase angle (ZPA). SS and SP are only able to operate either in CC mode with ZPA or CV mode with ZPA, but not in both [8]. Although [11] proposed a control system able to follow the CC-CV charging cycle for SP, it does not guarantee ZPA, which can be achieved by means of hybrid compensations [12]. By increasing the number of components, with a double side inductor-capacitor-capacitor (LCC-LCC) it is possible to fulfill both the CC-CV reference profiles and the ZPA condition. On the other hand, it requires many components, leading to an increase in size, power losses and control system complexity. The latter method becomes meaningless when the self-inductance of the primary side differs from the secondary one [8]. Also, the multiple-input-multiple-output (MIMO) configuration can be adopted in automotive applications. Reference [13] proposes a general design procedure, valid for any strictly-passive multi-port network, based on optimal impedance terminations for efficiency maximization. The efficiency can also be maximized for resonance frequency mismatch [14] or estimated using numerical and circuit models [15]. Multicoil systems have been also proposed in [16,17] to extend the transmission region and thus overcome the problem of the misalignment between the GA and VA coils, which can lead to severe components stress and disturbances [18–20], besides hazard magnetic fields [21,22]. However, when referring to automotive apparatuses, the size and weight of the components are fundamental parameters that have to be minimized. Regardless of the primary side topology, the parallel secondary compensation exhibits a much lower secondary self-inductance, when compared to the series one [23] and therefore it is preferred for automotive applications. Besides, all the above-mentioned papers consider the primary and secondary self-inductances of the resonant tank as input values, therefore they are not optimized for the target application.

This paper aims at providing a general design procedure, including the coil design, based on maximizing the tank efficiency and minimizing the VA self-inductance, considering the SP compensation network topology for automotive battery charging applications.

The structure of this manuscript is organized as follows: Section 2 provides two different design procedures based on analytical formulas, which have been tested on a case study described in Section 3. Finally, Section 4 concludes this paper discussing the results and possible future work.

2. Design Procedure

The design and tailoring of inductive couplers should be coordinated with both the compensation topology and the type of load, since both of them contribute to the overall system efficiency. The main goal is the transmission of the desired power through a certain control strategy based on load requirements, minimization of losses and optimization of system efficiency, coil size and weight. Figure 2 illustrates the adopted design procedure step by step taking into account the following points:

- SP compensation network
- Maximize the system efficiency
- Lightweight vehicle assembly
- Fulfil the required voltage gain
- Zero voltage switching (ZVS)
- Minimize the circulation of reactive power

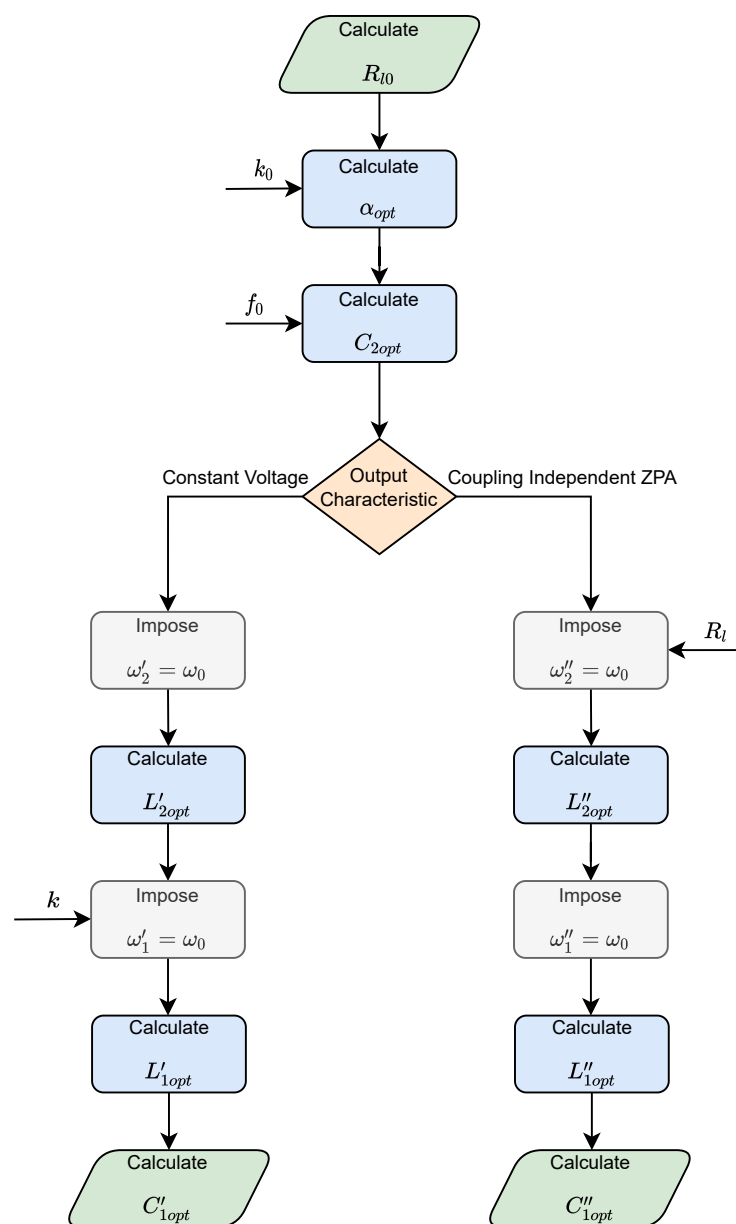


Figure 2. Flow chart illustrating the design algorithm for the inductive coupling and the compensation networks based on the selected output characteristic. The load resistance R_l and the coupling coefficient k refer to actual parameters during variable operating conditions.

The first design step consists in modelling the load by means of a proper equivalent resistance R_l , as discussed in Section 2.1. Then, a reference value R_{l0} for the load equivalent resistance must be chosen. The same holds for the coupling coefficient k between the GA and VA coils, which is generally defined as:

$$k = \frac{M}{\sqrt{L_1 L_2}} \quad (1)$$

where L_1 and L_2 are the self-inductance coefficients of the GA and VA windings, respectively, while M is their mutual inductance coefficient. A reference coupling coefficient value k_0 must be considered for the design. Once R_{l0} and k_0 are defined, the design passes through the choice of the secondary capacitor C_2 . Straightforwardly, the secondary inductor L_2 can be sized to make the receiver resonate at the desired frequency f_0 . Two different design procedures are proposed for achieving either a CV or ZPA at the desired resonant frequency. Pole splitting and bifurcation phenomena can be avoided deviating the proposed design rule for the inductance of about 15–20% [24]. Once the receiver parameters have been found, the primary inductance L_1 can be designed according to the desired voltage gain of the converter, which is defined as:

$$\hat{G}_v = \frac{\hat{V}_2}{\hat{V}_1} \quad (2)$$

with \hat{V}_1 and \hat{V}_2 the phasors associated to the input and output voltages of the inductive link $v_1(t)$ and $v_2(t)$, respectively, as depicted in Figure 3. This parameter clearly depends on the particular primary compensation network and its tuning. The lumped capacitor C_1 connected in series to L_1 is usually designed to make the input impedance of the inductive coupling purely real at the design resonant frequency f_0 .

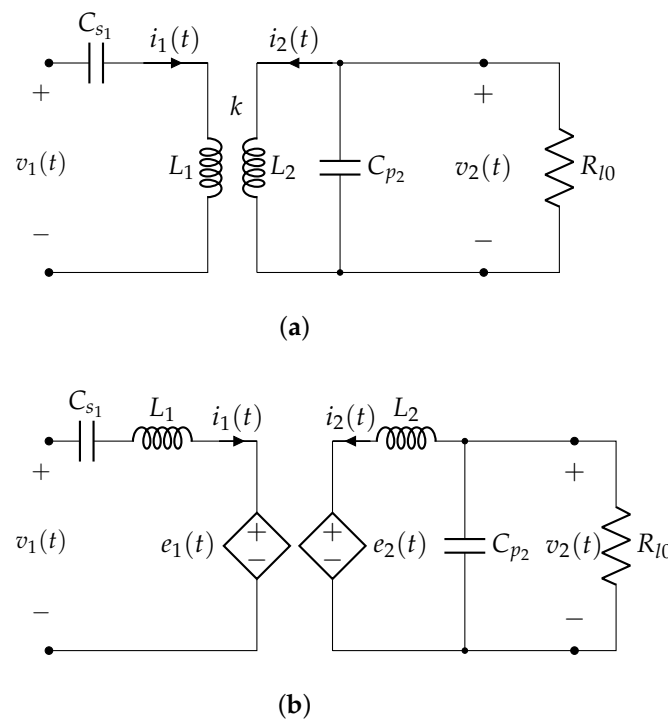


Figure 3. Equivalent circuits of the resonant inductive link where the inductive coupling is represented by means of (a) two coupled inductors and (b) two decoupled inductors with series controlled voltage sources.

2.1. Load Modelling

For battery charging applications, the load of the inductive link comprises a full-bridge diode rectifier followed by a second order filter, which feeds the DC link of the DC/DC converter that regulates the battery current and voltage. According to [25], in the hypothesis of ideal components, the overall load circuit seen at the terminals of the secondary side can be considered as an equivalent resistance defined as:

$$R_l = \frac{\pi^2}{8} \frac{V_{dc}^2}{P_{dc}} \quad (3)$$

where V_{dc} is the chopper DC link voltage and P_{dc} the power delivered to the battery.

2.2. Load Matching

According to [26], a total link efficiency can be defined as:

$$\eta_{T_{link}} = \frac{P_{load}}{P_{in_{link}}} = \frac{\frac{|\hat{V}_2|^2}{R_l}}{\text{Re} \left[\hat{V}_{L_1} \hat{I}_{L_1}^* \right]} \quad (4)$$

where \hat{V}_{L_1} is the phasor voltage across the primary coil L_1 and \hat{I}_{L_1} its phasor current. After some mathematical manipulations, it can be rewritten as:

$$\eta_{T_{link}} = \frac{k^2 Q_1 Q_2^2}{(\alpha + Q_2) \left(1 + k^2 Q_1 Q_2 + \frac{Q_2}{\alpha} \right)} \quad (5)$$

where Q_1 and Q_2 are the quality factors of the primary and secondary coils, respectively, k_0 the coupling coefficient between the primary and secondary coil and $\alpha = \omega C_2 R_l$ with $\omega = 2\pi f$ the angular frequency associated to the operating frequency f . This expression does not consider the primary compensation and thus it is valid for any topology. Moreover, no hypothesis has been done on the tuning of the receiver resonant frequency, which can be arbitrarily chosen, as it is discussed later on. Assuming high values of the quality factors Q_1 and Q_2 , for given k and R_l it is possible to find the optimum value of secondary-capacitive admittance ωC_2 that maximises the efficiency. It is obtained enforcing

$$\frac{\partial \eta_{T_{link}}}{\partial \alpha} = 0 \quad (6)$$

that leads to the following optimum value of α , considering the reference coupling coefficient k_0 :

$$\alpha_{opt} = \frac{Q_2}{\sqrt{1 + k_0^2 Q_1 Q_2}}. \quad (7)$$

Then, at the design resonant frequency f_0 , the optimum capacitance value for a reference load R_{l0} results:

$$C_{2_{opt}} = \frac{\alpha_{opt}}{\omega_0 R_{l0}}. \quad (8)$$

2.3. Design for Constant Voltage Output

A SP compensated resonant inductive link can achieve constant output voltage at the chosen ω_0 and coupling coefficient k_0 when designed such that:

$$\omega'_1 = \omega'_2 = \omega_0 \quad (9)$$

where:

$$\omega'_1 = \frac{1}{\sqrt{L_1 C_1 (1 - k_0^2)}} \quad \text{and} \quad \omega'_2 = \frac{1}{\sqrt{L_2 C_2}} \quad (10)$$

with L_1 and L_2 the self-inductances of the GA and VA coils, respectively, and C_1 and C_2 the lumped capacitances of the GA and VA compensation networks, respectively. Then, the optimal value of L_2 can be obtained from (9) considering (8) as:

$$L'_{2_{opt}} = \frac{1}{\omega_0^2 C_{2_{opt}}} \quad (11)$$

or, equivalently,

$$L'_{2_{opt}} = \frac{1}{\alpha_{opt}} \frac{R_{l0}}{\omega_0}. \quad (12)$$

For this configuration, the voltage gain can be written as:

$$|\hat{G}'_v| = \sqrt{\frac{L_2}{L_1} \left[\frac{\alpha Q_1 k_0}{1 + \alpha Q_1 k_0^2} \right]}. \quad (13)$$

The optimal value of the primary inductance can be matched considering the condition of maximum efficiency of the inductive link, for which the voltage gain can be rearranged introducing α_{opt} . After some mathematical manipulations, it holds:

$$\begin{aligned} L'_{1_{opt}} &= L'_{2_{opt}} \left(\frac{1}{|\hat{G}'_v|} \frac{\alpha_{opt} Q_1 k_0}{1 + \alpha_{opt} Q_1 k_0^2} \right)^2 \\ &= L'_{2_{opt}} \left(\frac{1}{|\hat{G}'_v|} \frac{k_0 Q_1 Q_2}{k_0^2 Q_1 Q_2 + \sqrt{1 + k_0^2 Q_1 Q_2}} \right)^2. \end{aligned} \quad (14)$$

The only missing component is the primary capacitor, which can be easily designed as:

$$C'_{1_{opt}} = \frac{1}{\omega_0^2 L'_{1_{opt}} (1 - k_0^2)}. \quad (15)$$

2.4. Design for Coupling Independent ZPA

While the design of compensation networks described in (9) allows CV operations, it does not allow the imaginary part of the receiver impedance to be completely cancelled. The basic idea behind resonant circuits is to reduce the amount of reactive power required by the circuit for a fixed active power. It corresponds to eliminate the imaginary component of the circuit impedance, which is, in this case, the impedance seen by the (ideal) controlled voltage source $e_2(t)$ representing the secondary induced voltage, as it can be seen in Figure 3b. For a receiver with parallel compensation, the impedance can be expressed as:

$$\hat{Z}_2 = R_2 + j\omega L_2 + \frac{R_{l0}}{1 + j\omega C_2 R_{l0}} \quad (16)$$

$$= R_2 + \frac{1}{1 + (\omega C_2 R_{l0})^2} + j\omega \left(L_2 - \frac{C_2 R_{l0}^2}{1 + (\omega C_2 R_{l0})^2} \right) \quad (17)$$

and thus it is possible to have $\text{Im}[\hat{Z}_r] = 0$ at ω_0 if:

$$\omega_2'' = \sqrt{\frac{C_2 R_l - L_2}{L_2 C_2^2 R_{l0}^2}} = \omega_0. \quad (18)$$

However, it should be noticed that \hat{Z}_2 presents a “residual” real term, which is due to the particular compensation topology and cannot be cancelled. The ideal receiver impedance can be considered the pure load R_{l0} , but this condition can be achieved only with an imaginary resonant frequency, which is, of course, meaningless. From (18), it is possible to find the optimal secondary inductance value at ω_0 as:

$$L''_{2_{opt}} = \frac{C_{2_{opt}} R_{l0}^2}{1 + (\omega_0 C_{2_{opt}} R_{l0})^2} \quad (19)$$

or, equivalently,

$$L''_{2_{opt}} = \frac{\alpha_{opt}}{1 + \alpha_{opt}^2} \frac{R_{l0}}{\omega_0}. \quad (20)$$

In case the receiver is tuned according to (18), a real input impedance simply requires L_1 and C_1 to be sized such that:

$$\omega''_1 = \frac{1}{\sqrt{L_1 C_1}} = \omega_0. \quad (21)$$

In this condition, the voltage gain amplitude results:

$$|\hat{G}_v''| = \sqrt{\frac{L_2}{L_1}} \frac{k Q_1 Q_2 \sqrt{\alpha^2 + 1}}{\alpha k^2 Q_1 Q_2 + \alpha + Q_2^2}. \quad (22)$$

Introducing α_{opt} it leads to an optimal primary inductance value defined as:

$$\begin{aligned} L''_{1_{opt}} &= L''_{2_{opt}} \left(\frac{k_0 Q_1 Q_2 \sqrt{\alpha_{opt}^2 + 1}}{|\hat{G}_v''| (\alpha_{opt} k_0^2 Q_1 Q_2 + \alpha_{opt} + Q_2^2)} \right)^2 \\ &= L''_{2_{opt}} \left(\frac{k_0 Q_1 \sqrt{\frac{1+k_0^2 Q_1 Q_2 + Q_2^2}{1+k_0^2 Q_1 Q_2}}}{|\hat{G}_v''| (1 + \sqrt{1 + k_0^2 Q_1 Q_2})} \right)^2 \end{aligned} \quad (23)$$

and thus the primary capacitor can be sized as:

$$C''_{1_{opt}} = \frac{1}{\omega_0^2 L''_{1_{opt}}}. \quad (24)$$

3. Case Study

The design procedures presented in the previous section are applied to a real test case, made of a battery pack and a charging system for automotive applications. The specifications required for the inductive link design are given in the first part of Table 1, while the second and third part list the inductive link components. To start the procedure, the required design guesses are:

- Inductor quality factors Q_1 and Q_2 ;
- Reference coupling coefficient k_0 .

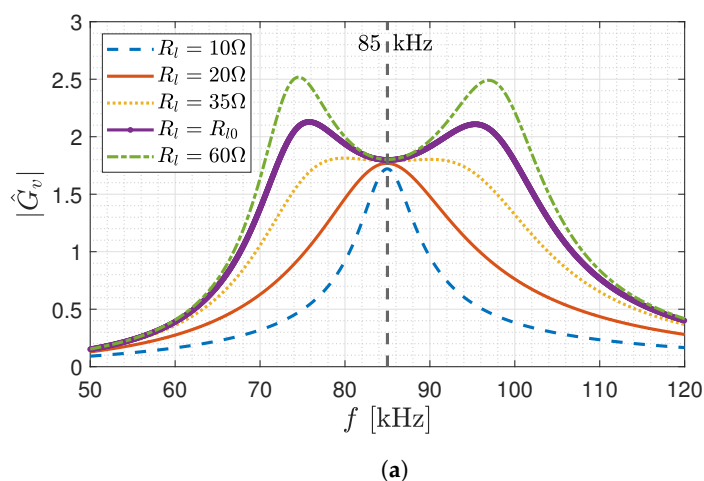
For both the proposed design procedures, the secondary inductance L_2 results about four times lower with respect to the primary one L_1 , confirming the theoretical predictions. Moreover, the comparison between (12) and (20) suggests that the tuning method proposed in (18) leads to a smaller secondary inductance, for given values of R_l , ω_0 and k_0 . In addition, studying the trends of $L'_{2_{opt}}$ and $L''_{2_{opt}}$ as a function of α it can be found that the two inductances present approximately the same value for $\alpha_{opt} > 4$, regardless of the particular system specifications.

Table 1. Case study system parameters.

Quantity	Symbol	Value	Unit of Measure
Specifications			
On board DC bus rated voltage	V_{dc}	420	V
Inverter DC bus rated voltage	V_{DC}	230	V
Power rate	P_{dc}	3	kW
Operating frequency	f_0	85	kHz
Primary inductor quality factor	Q_1	$\gg 100$	-
Secondary inductor quality factor	Q_2	$\gg 100$	-
Reference coupling coefficient	k_0	0.3	-
CV Output—Optimal Design at $\omega_0 = \omega'_1 = \omega'_2$			
Primary inductor	L'_{1opt}	89.8	uH
Secondary inductor	L'_{2opt}	26.77	uH
Primary capacitor	C'_{1opt}	43	nF
Secondary capacitor	C'_{2opt}	131	nF
ZPA Output—Optimal Design at $\omega_0 = \omega''_1 = \omega''_2$			
Primary inductor	L''_{1opt}	89.8	uH
Secondary inductor	L''_{2opt}	24.5	uH
Primary capacitor	C''_{1opt}	42.9	uF
Secondary capacitor	C''_{2opt}	131	uF

The main difference between the two design procedures can be understood by means of the analytical formulas reported in Section 2 and it can be graphically visualized in Figures 4–6. In particular, Figures 4a and 5a show the magnitude of the voltage gain as a function of the frequency for different loads. Figure 4a clearly indicates that the voltage gain is nearly constant at the chosen ω_0 , with the compensation network parameters tuned according to (9). Reversely, in case of $\omega''_1 = \omega''_2 = \omega_0$, Figure 5a highlights that the voltage gain magnitude at ω_0 varies depending on the load, especially for low values of R_l .

The input impedance angle defines the effective reactive demand of the WPT link and the possibility of ZVS operations. It is plotted in Figures 4b and 5b as a function of the frequency and for different loads for a system designed such that $\omega_0 = \omega'_1 = \omega'_2$ and $\omega_0 = \omega''_1 = \omega''_2$, respectively. At ω_0 , the former tuning allows ZPA operations for any load, while in the latter case they are possible only if $R_l = R_{l0}$. This can be explained considering the definition of the system angular frequency, which is independent on the load for ω'_1 and ω'_2 , whereas the value of ω''_2 is affected by R_l .

**Figure 4.** Cont.

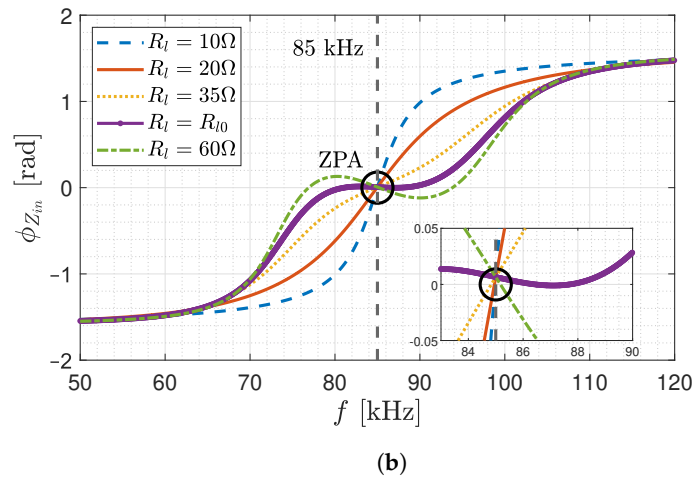


Figure 4. (a) Voltage gain magnitude and (b) input impedance angle as a function of the frequency for the inductive link designed for working with CV operations at $f_0 = 85$ kHz.

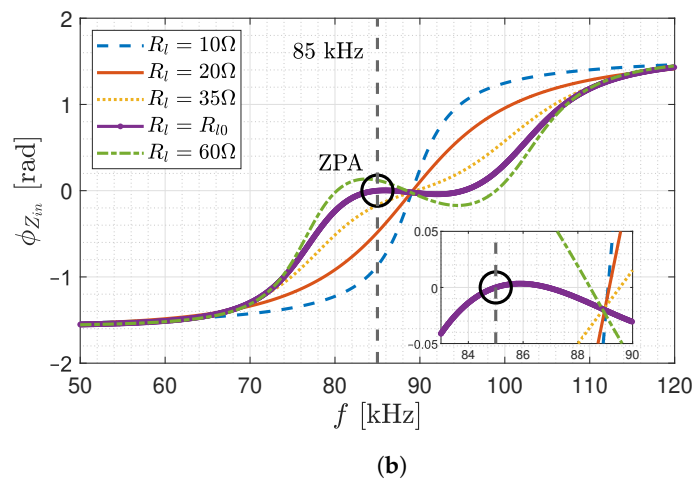
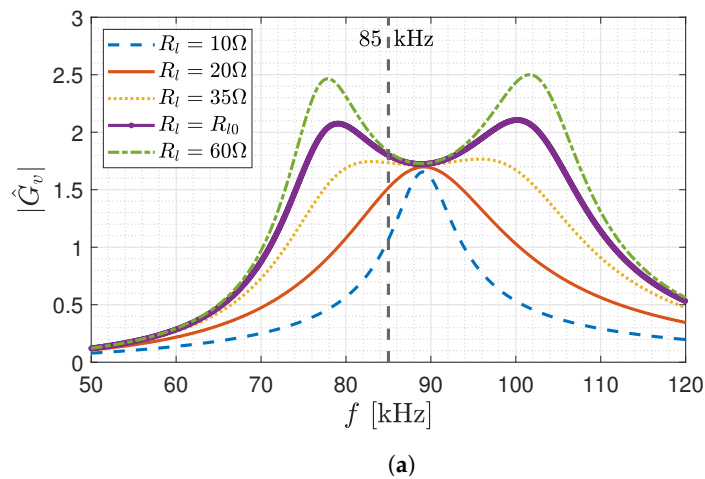


Figure 5. (a) Voltage gain magnitude and (b) input impedance angle as a function of the frequency for the inductive link designed for coupling independent ZPA operations at $f_0 = 85$ kHz.

Another crucial parameter that affects the behaviour of the WPT link is the coupling coefficient k , which basically depends on the alignment between the GA and VA coils. The trends of the input impedance angles as a function of the frequency for different values of the coupling coefficient for $\omega_0 = \omega'_1 = \omega'_2$ and $\omega_0 = \omega''_1 = \omega''_2$ are plotted in Figure 6a,b, respectively. ZPA operations at ω_0 are possible for any coupling coefficient only in the latter

case, since k does not appear in the definition of ω_1'' and ω_2'' . In the case of $\omega_0 = \omega_1' = \omega_2'$, the input impedance angle depends on the alignment condition between the VA and GA coils, being positive for $k < k_0$ and negative for $k > k_0$.

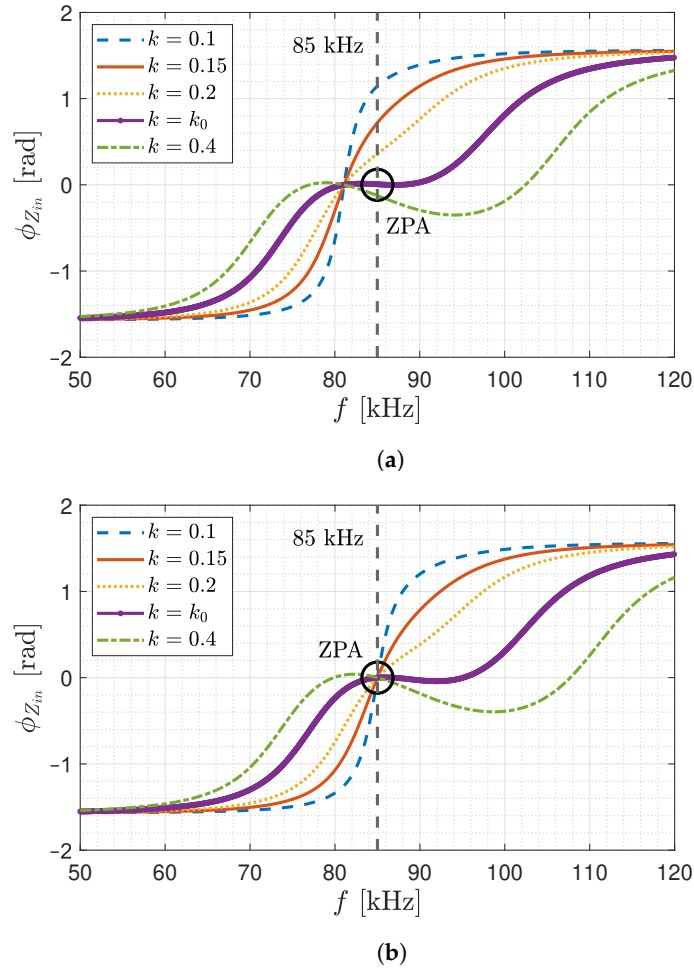


Figure 6. Input impedance angle as a function of the frequency for different coupling coefficients in case of inductive link designed for (a) CV output and (b) coupling independent ZPA operations at $f_0 = 85$ kHz.

Efficiency Characterization

In order to validate the proposed design procedures, the efficiency of the SP compensated WPT link, whose parameters are listed in Table 1, has been calculated for different operating conditions. Figure 7 represents, in logarithmic scale, the efficiency calculated unless iron and diodes losses as a function of the equivalent load resistance R_l for different coupling coefficients k , for a system designed for CV or coupling independent ZPA. The operating frequency is $f_0 = 85$ kHz. Overall, Figure 7 shows that for a certain value of R_l the efficiency is higher as the coupling coefficient increases, while the maximum of the efficiency curve occurs in correspondence of higher equivalent loads as the coupling coefficient decreases. In general, the tuning for coupling independent ZPA, namely for $\omega_0 = \omega_1'' = \omega_2''$, guarantees a slightly higher efficiency with respect to the tuning for CV operations, obtained with $\omega_0 = \omega_1' = \omega_2'$. This is due to the tuning of the secondary capacitor, which perfectly cancels the imaginary part of the receiver impedance only if $\omega_0 = \omega_1'' = \omega_2''$. However, as expected, for $R_l = R_{l0}$, the systems designed for CV and coupling independent ZPA operations present the same efficiency, and this occurs for any k . In particular, for $k = k_0$, the efficiency at $R_l = R_{l0}$ is maximum, with a value of 97.8%. The main difference between the efficiency trends, resulting from the two different design

procedures, is more evident for high equivalent loads, where the curves obtained with the CV design overlap, unlike the ones resulting from the coupling independent ZPA design.

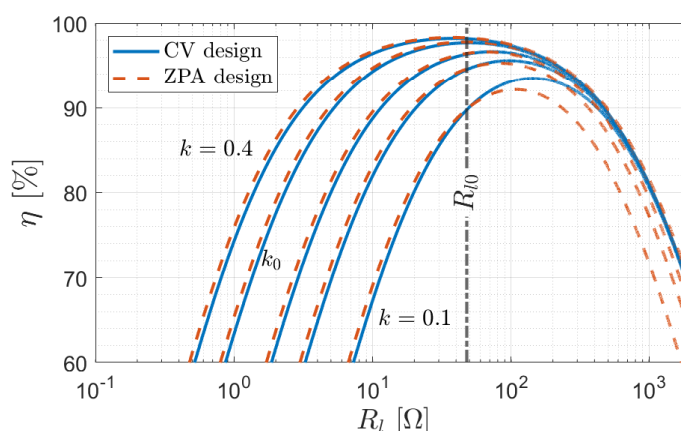


Figure 7. Overall link efficiency of a WPT system designed for CV or coupling independent ZPA, operating at f_0 , as a function of the receiver equivalent load R_l , for different coupling coefficients k .

4. Conclusions

Despite the resulting values of the inductive link parameters are quite similar, this analysis has highlighted that the behaviour of the system for different load and coupling coefficient values is different. For a given operating frequency, it is possible to achieve CV operations in ZPA conditions for any receiver load. However, at that frequency, the input impedance strongly varies depending on the coupling coefficient, preventing ZPA operations with a consequent drop of the system efficiency. Reversely, an alternative tuning able to ensure constant ZPA operations at the chosen resonant frequency is possible, with the drawbacks of load-dependent voltage gain and input impedance angle. Moreover, this tuning allows the perfect compensation of the receiver impedance \hat{Z}_2 reducing the reactive power demand. At a certain induced voltage, it experiences lower current, with a consequent increase in the efficiency. This is confirmed by the efficiency analysis, which also verified that, for $k \approx k_0$, efficiency values of about 97.5% are guaranteed for a wide range of loads R_l . As expected, the secondary inductance results much smaller than the primary one, meaning that the VA coil is much lighter than the GA one. Overall, both the proposed compensations present pros and cons and thus they have to be chosen depending on the target application.

Author Contributions: Conceptualization, M.S. and A.C.; methodology, M.S. and A.C.; software, A.C. and M.S.; investigation, M.S. and A.C.; resources, M.S.; writing—original draft preparation, M.S. and A.C.; writing—review and editing, M.S., A.C., L.S. and C.R.; supervision, L.S. and C.R. All authors have read and agreed to the published version of the manuscript.

Funding: This research received no external funding.

Institutional Review Board Statement: Not applicable.

Informed Consent Statement: Not applicable.

Data Availability Statement: Data is available in the paper.

Conflicts of Interest: The authors declare no conflict of interest.

References

1. Covic, G.A.; Boys, J.T. Modern Trends in Inductive Power Transfer for Transportation Applications. *IEEE J. Emerg. Sel. Top. Power Electron.* **2013**, *1*, 28–41. [[CrossRef](#)]
2. Li, S.; Mi, C.C. Wireless Power Transfer for Electric Vehicle Applications. *IEEE J. Emerg. Sel. Top. Power Electron.* **2015**, *3*, 4–17.
3. Patil, D.; McDonough, M.K.; Miller, J.M.; Fahimi, B.; Balsara, P.T. Wireless Power Transfer for Vehicular Applications: Overview and Challenges. *IEEE Trans. Transp. Electrification* **2017**, *4*, 3–37. [[CrossRef](#)]

4. She, C.; Zhang, L.; Wang, Z.; Sun, F.; Liu, P.; Song, C. Battery State of Health Estimation Based on Incremental Capacity Analysis Method: Synthesizing from Cell-Level Test to Real-World Application. *IEEE J. Emerg. Sel. Top. Power Electron.* **2021**. [CrossRef]
5. Wang, Z.; Song, C.; Zhang, L.; Zhao, Y.; Liu, P.; Dorrell, D.G. A Data-Driven Method for Battery Charging Capacity Abnormality Diagnosis in Electric Vehicle Applications. *IEEE Trans. Transp. Electr.* **2021**. [CrossRef]
6. Zhang, W.; Mi, C.C. Compensation topologies of high-power wireless power transfer systems. *IEEE Trans. Veh. Technol.* **2016**, *65*, 4768–4778. [CrossRef]
7. Aditya, K.; Williamson, S.S. Comparative study of Series-Series and Series-Parallel compensation topologies for electric vehicle charging. In Proceedings of the IEEE 23rd International Symposium on Industrial Electronics (ISIE), Istanbul, Turkey, 1–4 June 2014; pp. 426–430.
8. Vu, V.B.; Tran, D.H.; Choi, W. Implementation of the Constant Current and Constant Voltage Charge of Inductive Power Transfer Systems With the Double-Sided LCC Compensation Topology for Electric Vehicle Battery Charge Applications. *IEEE Trans. Power Electron.* **2018**, *33*, 7398–7410. [CrossRef]
9. Huang, Z.; Wong, S.C.; Tse, C.K. Design methodology of a series-series inductive power transfer system for electric vehicle battery charger application. In Proceedings of the IEEE Energy Conversion Congress and Exposition (ECCE), Pittsburgh, PA, USA, 14–18 September 2014; pp. 1778–1782.
10. Zhang, W.; Wong, S.C.; Tse, C.K.; Chen, Q. Design for Efficiency Optimization and Voltage Controllability of Series-Series Compensated Inductive Power Transfer Systems. *IEEE Trans. Power Electron.* **2014**, *29*, 191–200. [CrossRef]
11. Simonazzi, M.; Campanini, A.; Sandrolini, L.; Rossi, C. Single Stage Wireless Power Transfer Battery Charger for Electric Vehicles. In Proceedings of the IEEE 15th International Conference on Compatibility, Power Electronics and Power Engineering (CPE-POWERENG), Florence, Italy, 14–16 July 2021; pp. 1–6.
12. Mai, R.; Chen, Y.; Li, Y.; Zhang, Y.; Cao, G.; He, Z. Inductive Power Transfer for Massive Electric Bicycles Charging Based on Hybrid Topology Switching With a Single Inverter. *IEEE Trans. Power Electron.* **2017**, *32*, 5897–5906. [CrossRef]
13. Monti, G.; Mongiardo, M.; Minnaert, B.; Costanzo, A.; Tarricone, L. Multiple Input Multiple Output Resonant Inductive WPT Link: Optimal Terminations for Efficiency Maximization. *Energies* **2021**, *14*, 2194. [CrossRef]
14. Stankiewicz, J.M.; Choroszucho, A.; Steckiewicz, A. Estimation of the Maximum Efficiency and the Load Power in the Periodic WPT Systems Using Numerical and Circuit Models. *Energies* **2021**, *14*, 1151. [CrossRef]
15. Weerasekara, H.; Hata, K.; Imura, T.; Fujimoto, H.; Hori, Y. Efficiency Maximization in Wireless Power Transfer Systems for Resonance Frequency Mismatch. In Proceedings of the IEEE PELS Workshop on Emerging Technologies: Wireless Power Transfer (WoW), London, UK, 18–21 June 2019; pp. 363–366.
16. Pakhaliuk, B.; Shevchenko, V.; Mućko, J.; Husev, O.; Lukianov, M.; Kołodziejek, P.; Strzelecka, N.; Strzelecki, R. Optimal Rotating Receiver Angles Estimation for Multicoil Dynamic Wireless Power Transfer. *Energies* **2021**, *14*, 6144. [CrossRef]
17. Simonazzi, M.; Sandrolini, L.; Zarri, L.; Reggiani, U.; Alberto, J. Model of Misalignment Tolerant Inductive Power Transfer System for EV Charging. In Proceedings of the IEEE 29th International Symposium on Industrial Electronics (ISIE), Delft, The Netherlands, 17–19 June 2020; pp. 1617–1622.
18. Campi, T.; Cruciani, S.; Maradei, F.; Feliziani, M. Conducted emission of wireless power transfer charging system in electric vehicle. In Proceedings of the IEEE International Symposium on Electromagnetic Compatibility, Washington, DC, USA, 7–11 August 2017; pp. 619–622.
19. Spadacini, G.; Grassi, F.; Pignari, S.A. Modelling and simulation of conducted emissions in the powertrain of electric vehicles. *Prog. Electromagn. Res. B* **2016**, *69*, 1–15. [CrossRef]
20. Simonazzi, M.; Sandrolini, L. Conducted Emission Analysis of a Near-Field Wireless Power Transfer System. In Proceedings of the IEEE 15th International Conference on Compatibility, Power Electronics and Power Engineering (CPE-POWERENG), Florence, Italy, 14–16 July 2021; pp. 1–6.
21. 16ENG08 EMPIR MICEV Consortium. *Best Practice Guide for the Assessment of EMF Exposure from Vehicle Wireless Power Transfer Systems*; Guilizzoni, R., Harmon, S., Zucca, M., Eds.; 17 February 2021. Available online: <https://hal.archives-ouvertes.fr/hal-03312964/document> (accessed on 5 November 2021)
22. Cruciani, S.; Campi, T.; Maradei, F.; Feliziani, M. Active Shielding Design and Optimization of a Wireless Power Transfer (WPT) System for Automotive. *Energies* **2020**, *13*, 5575. [CrossRef]
23. Bosshard, R.; Kolar, J.W.; Mühlethaler, J.; Stevanović, I.; Wunsch, B.; Canales, F. Modeling and η - α -pareto optimization of inductive power transfer coils for electric vehicles. *IEEE J. Emerg. Sel. Top. Power Electron.* **2015**, *3*, 50–64. [CrossRef]
24. Wang, C.S.; Covic, G.; Stielau, O. Power transfer capability and bifurcation phenomena of loosely coupled inductive power transfer systems. *IEEE Trans. Ind. Electron.* **2004**, *51*, 148–157. [CrossRef]
25. Steigerwald, R.L. A Comparison Of Half-Bridge Resonant Converter Topologies. *IEEE Trans. Power Electron.* **1988**, *3*, 174–182. [CrossRef]
26. Schuylenbergh, K.V.; Puers, R. *Inductive Powering: Basic Theory and Application to Biomedical Systems*, 1st ed.; Springer Science: Berlin, Germany, 2009.